Interplay of effects of neutron skins in coordinate space and proton skins in momentum space on emission of hard photons in heavy-ion collisions near the Fermi energy

Wen-Mei Guo [1,*] Bao-An Li [2,†] and Gao-Chan Yong[3,‡]
[1]*Department of Physics, Anhui Normal University, Wuhu 241000, China*
[2]*Department of Physics and Astronomy, Texas A&M University-Commerce, Commerce, Texas 75429-3011, USA*
[3]*Institute of Modern Physics, Chinese Academy of Sciences, Lanzhou 730000, China*

(Received 13 July 2023; accepted 7 September 2023; published 25 September 2023)

Within an isospin- and momentum-dependent Boltzmann-Uehling-Uhlenbeck transport model, we investigate the hard photons emission from neutron-proton bremsstrahlung in the reaction system of ^{208}Pb + ^{208}Pb around Fermi energy. Effects of neutron skins in coordinate (r) space and proton skins in momentum (k) space on the time evolution, the angular distribution, and the transverse momentum spectra of hard photons with different energies are studied. It is shown that the emission of direct hard photons is sensitive to the neutron skin, which has larger effects for more energetic hard photons. Meanwhile, we find that the proton skins have an important influence on the emission of direct hard photons, and its effect is actually even larger than that of neutron skins. It needs to take the effect of proton skins into account when we determine the size of neutron skins by comparing transport mode predictions of hard photons with the corresponding experimental measurements.

DOI: 10.1103/PhysRevC.108.034617

I. INTRODUCTION

For two decades, the neutron skin thickness of nuclei as a sensitive probe of the nuclear symmetry energy has attracted much attention in nuclear physics and astrophysics [1–4]. It is defined as the difference between the root-mean-square (rms) radii of neutrons and protons, i.e., $\Delta r_{np} = \langle r_n^2 \rangle^{1/2} - \langle r_p^2 \rangle^{1/2}$. Much effort has been devoted to measuring the size of neutron skin experimentally, e.g., photopion production, pionic and antiprotonic atoms method at CERN [5–7] and parity-violating electron scattering at the Jefferson Laboratory (PREX-I and PREX-II experiment) [8,9]. Theoretically, lots of theories, e.g., mean-field models [4,10], *ab initio* computations [11,12] and droplet models [3,13], have been used to study the neutron skin thicknesses of neutron-rich nuclei. Moreover, extractions of Δr_{np} in ^{208}Pb and ^{209}Bi from different hadronic probes have been made [14,15], although there might be some degree of model dependence involved. However, the community has not reached a consensus on precise values of neutron skins of heavy nuclei. Therefore, it is of great importance to improve the accuracy of the extraction of neutron skin thickness for helping us to explore the density dependence of nuclear symmetry energy, which is conducive to understanding properties of neutron-rich matter and even of neutron stars for us.

It is well known that observables of heavy-ion collisions are sensitive to the initial phase space distributions of nucleons or quarks and gluons in the colliding nuclei. For example, it was proposed that the yield ratios of a neutron-proton and that of ^{3}H - ^{3}He could serve as the sensitive probes to neutron skin thickness in heavy-ion collisions, see, e.g., Refs. [16,17] for recent reviews. The neutron skin effect also has been studied at both intermediate [18] and relativistic heavy-ion collisions [19–21]. It is also well known that hard photons are promising probes to study the reaction dynamics in nuclear physics [22], because they only interact weakly with the nuclear medium through an electromagnetic force unlike hadronic probes inevitably suffering from distortions due to strong interactions in the final stage. For hard photons, usually defined as γ-ray spectra above 30 MeV (distinct from the giant dipole resonance emission [23]), experimental and theoretical studies consistently indicate that they are emitted mainly in incoherent proton-neutron bremsstrahlung, $p + n \to p + n + \gamma$, during the early stages of heavy-ion collisions [24–28]. This part of hard photons associated with the first-chance proton-neutron collisions are called direct photons. Recently, Refs. [29,30] have put forward that hard photon emission can be taken as an experimental observable to extract information on neutron skin thickness. On the other hand, nucleon-nucleon short-range correlations (SRCs) due to the tensor components and/or the repulsive core of nuclear forces have attracted much attention in recent years [31–33]. The SRC will lead to the formation of a high-momentum tail (HMT) in the single-nucleon momentum distribution. Incorporating the SRC effects in the extended Thomas-Fermi model, Ref. [34] shows that proton skins in k space coexist with neutron skins in r space in heavy nuclei and their correlation is governed by Liouville's theorem and Heisenberg's uncertainty principle. Investigating SRC effects in nuclei, nuclear reactions, and neutron stars is a major task in nuclear physics [35].

*guowenmei@ahnu.edu.cn
†bao-an.li@tamuc.edu
‡yonggaochan@impcas.ac.cn

In the present work, the Thomas-Fermi approximation to the nucleon kinetic-energy density, which incorporates the SRC effects, was considered in the isospin- and momentum-dependent Boltzmann-Uehling-Uhlenbeck (IBUU) transport model. The interplay of effects of neutron skins in r space and proton skins in k space on hard photons emission in heavy-ion collisions around Fermi energy was studied.

II. THEORETICAL FRAMEWORK

In this study, we adopt the updated IBUU transport model which originated from the IBUU04 model [36,37]. The initial density distributions of nucleons in projectile and target are obtained from the two-parameter Fermi (2pF) distribution widely used in the literature, i.e.,

$$\rho_J(r) = \rho_0^J\{1 + \exp[(r - c_J)/a_J]\}^{-1}, \tag{1}$$

where c_J and a_J are the half-density radius and diffuseness parameter, respectively.

With the fact that the momentum distribution of nucleons has a high momentum tail due to SRCs, the parametrized nucleon momentum distribution according to Refs. [34,38] is taken into account in our IBUU model and given as follows:

$$n_k^J(\rho,\delta) = \begin{cases} \Delta_J, & 0 < |\mathbf{k}| < k_F^J, \\ C_J\left(k_F^J/|\mathbf{k}|^4\right), & k_F^J < |\mathbf{k}| < \phi_J k_F^J, \end{cases} \tag{2}$$

where k_F^J is the Fermi momentum of the nucleon J. The Δ_J denotes the depletion of the Fermi sea with respect to the step function for a free Fermi gas. The parameters Δ_J, C_J, and ϕ_J depend linearly on the isospin asymmetry $\delta = (\rho_n - \rho_p)/\rho$ in a general form of $Y_J = Y_0(1 + Y_1\tau_3^J\delta)$, where $\tau_3^n = +1$ and $\tau_3^p = -1$ [39–41]. The amplitude C_J and the high-momentum cutoff coefficient ϕ_J determine the fraction of nucleons in the HMT via $x_J^{\rm HMT} = 3C_J(1 - \phi_J^{-1})$. The above parameters are constrained by the the normalization condition $[2/(2\pi)^3]\int_0^\infty n_{\mathbf{k}}^J(\rho,\delta)d\mathbf{k} = (k_F^J)^3/3\pi^2$, the equation of state of pure neutron matter (PNM) from microscopic many-body theories [42–47] and the systematic analysis of many experiments about the percentage of nucleons in the HMT on the symmetry nuclear matter (SNM) [38,48,49]. According to Ref. [34], the HMT-exp parameters sets of $x_{\rm SNM}^{\rm HMT} = 28\%$, $x_{\rm PNM}^{\rm HMT} = 4\%$, which caused $C_0 = 0.161$, $C_1 = -0.25$, $\phi_0 = 2.38$, and $\phi_1 = -0.56$, were adopted in our study. With this nucleon momentum distribution, the proton skin was displayed in k space, and its thickness grows with the isospin asymmetry [34]. Effects of the SRC/HMT described above on nuclear symmetry energy and properties of neutron stars have been studied extensively. For a review, see, e.g., Ref. [50].

Incorporating the SRC effects in the extended Thomas-Fermi approximation, the nucleon kinetic-energy density profile in finite nuclei is modified as [34]

$$\varepsilon_J^{\rm kin}(r) = \frac{1}{2M}\left[\alpha_J^\infty\rho_J^{5/3}(r)\Phi_J + \frac{\eta_J}{36}\frac{[\nabla\rho_J(r)]^2}{\rho_J(r)} + \frac{1}{3}\Delta\rho_J(r)\right]. \tag{3}$$

The first term with $\alpha_J^\infty = (3/5)(3\pi^2)^{2/3}$ is the bulk part as if nucleons are in infinite nuclear matter, in which $\Phi_J = 1 + C_J(5\phi_J + 3/\phi_J - 8) > 1$ is determined by properties of the HMT. It makes the bulk part of the kinetic-energy density enhanced more for protons than neutrons in neutron-rich systems, since relatively more protons are depleted from the Fermi sea to form a proton skin in the HMT. Here, $\Phi_p = 2.09$ and $\Phi_n = 1.60$ was used for isospin asymmetry $\delta = 0.21$. The second term originally proposed by Weizsäcker [51] is called the surface term in this study as it is very sensitive to surface properties of finite nuclei. Its strength factor η_J has been under debate and was found to affect significantly the halo and skin nature of the surfaces of heavy nuclei [34,52,53]. It can be constrained using the experimental information of the density profile and the average kinetic energy $\langle E_J^{\rm kin}\rangle$ of nucleons. The third term relating to the Laplacian operator is very small because of the smooth nuclear surface.

We adopt the same formalism from Ref. [34] for the proton skin in k space, which is similar to the measure of the neutron skin in r space ($\Delta r_{np} = \langle r_n^2\rangle^{1/2} - \langle r_p^2\rangle^{1/2}$ with $\langle r_{n/p}^2\rangle^{1/2}$ the rms radius of neutrons or protons), that is the difference between the average kinetic energies of protons and neutrons, i.e., $\Delta E_{pn}^{\rm kin} \equiv \langle E_p^{\rm kin}\rangle - \langle E_n^{\rm kin}\rangle$ with

$$\left\langle E_J^{\rm kin}\right\rangle = \int_0^\infty \varepsilon_J^{\rm kin}(r)d\mathbf{r}\Big/\int_0^\infty \rho_J(r)d\mathbf{r} \equiv \left\langle k_J^2\right\rangle/2M, \tag{4}$$

In this study, the following isospin- and momentum-dependent mean field single-nucleon potential is used [54],

$$\begin{aligned} U(\rho,\delta,\mathbf{p},\tau) = {} & A_u(x)\frac{\rho_{\tau'}}{\rho_0} + A_l(x)\frac{\rho_\tau}{\rho_0} \\ & + B\left(\frac{\rho}{\rho_0}\right)^\sigma(1 - x\delta^2) - 8x\tau\frac{B}{\sigma+1}\frac{\rho^{\sigma-1}}{\rho_0^\sigma}\delta\rho_{\tau'} \\ & + \frac{2C_{\tau,\tau}}{\rho_0}\int d^3\,\mathbf{p}'\frac{f_\tau(\mathbf{r},\mathbf{p}')}{1 + (\mathbf{p} - \mathbf{p}')^2/\Lambda^2} \\ & + \frac{2C_{\tau,\tau'}}{\rho_0}\int d^3\,\mathbf{p}'\frac{f_{\tau'}(\mathbf{r},\mathbf{p}')}{1 + (\mathbf{p} - \mathbf{p}')^2/\Lambda^2}, \end{aligned} \tag{5}$$

where $\tau = 1/2$ $(-1/2)$ for neutrons (protons), $\delta = (\rho_n - \rho_p)/(\rho_n + \rho_p)$ is the isospin asymmetry, and ρ_n, ρ_p denote neutron and proton densities, respectively. Specifically, the parameters $A_u(x)$, $A_l(x)$, B, $C_{\tau,\tau}$, $C_{\tau,\tau'}$ σ, and Λ with SRCs are updated by fitting empirical nature of nuclear matter, for example, the saturation density $\rho_0 = 0.16$ fm^{-3}, the binding energy $E_0 = -16$ MeV, the incompressibility $K_0 = 230$ MeV, and the isoscalar effective mass $m_s^* = 0.7m$ and so on. $f_\tau(\mathbf{r},\mathbf{p})$ is the phase-space distribution function at coordinate $\mathbf{r}$ and momentum $\mathbf{p}$. Different x parameters can be used to mimic different forms of the symmetry energy predicted by various many-body theories without changing any property of the symmetric nuclear matter and the symmetry energy at normal density. And for nucleon-nucleon scattering, the isospin-dependent reduced in-medium nucleon-nucleon cross section is adopted.

Hard photons production in heavy-ion reactions at intermediate energy has been studied theoretically and experimentally in a number of works [22,26,28,55–59]. Although the elementary cross section for the $p + n \to p + n + \gamma$ process is still model dependent [24,60–62], the calculations from theoretical reaction models are able to reasonably reproduce all qualitative features of the hard photon experimental data [55]. In this

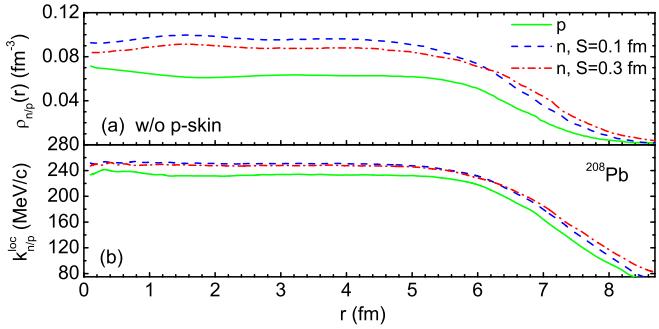

FIG. 1. Input local density (a) and calculated momentum profiles (b) for nucleons in ^{208}Pb and for neutrons with neutron skin thicknesses $S = 0.1$ fm and $S = 0.3$ fm. In this case the nucleon kinetic-energy density of colliding nuclei just includes the bulk part.

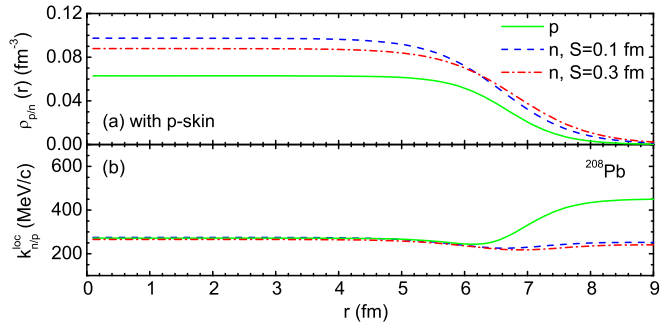

FIG. 2. Same with Fig. 1, but considering the surface term in the nucleon kinetic-energy density of colliding nuclei.

work, we adopt the following approach for the probability of hard photons production based on the neutral scalar σ meson exchange model by standard quantum field theory [24], in which more quantum mechanical effects was considered. It is fitted by an analytical expression:

$$\frac{d^2p_\gamma}{d\Omega dE_\gamma} = 1.671\times10^{-7}\frac{(1-y^2)^\alpha}{y}, \tag{6}$$

where $y = E_\gamma/E_{\max}$, $\alpha = 0.7319 - 0.5898\beta_i$, E_γ is energy of emitted photon, $E_{\max}$ is the total energy available in the proton-neutron c.m. system, β_i is the nucleon initial velocity. In the program, the effects of Pauli blocking in final state at the $p + n \to p + n + \gamma$ process are also taken into account [26]. The emissions of photons here are assumed to be isotropic in the proton-neutron c.m. frame, therefore one obtains the single differential elementary probability of the photon by averaging the solid angle over 4π, i.e.,

$$p_\gamma = \frac{dN}{dE_\gamma} = 2.1\times10^{-6}\frac{(1-y^2)^\alpha}{y}. \tag{7}$$

III. RESULTS AND DISCUSSIONS

As a comparison, we calculate the initial density distribution of nucleons in colliding nuclei from the Skyrme-Hartree-Fock calculations with the Skyrme M^* parameter set [63] used in the IBUU model before. And the parametrized nucleon momentum distribution which includes the HMT mentioned above has been adopted. Shown in Fig. 1 is the nucleons' average local density (a) and momentum (b) as a function of radius r in ^{208}Pb. The solid line represents protons. The dashed line and dash dotted line are for neutrons with neutron skin thicknesses $S = 0.1$ fm and $S = 0.3$ fm, respectively. The momentum profiles in Fig. 1(b) are calculated from Eq. (4) in which the nucleon kinetic-energy density just includes the bulk part. We can see that neutrons have higher local momenta due to their higher densities than protons in the entire radius area of ^{208}Pb. However, the protons have higher local momenta than neutrons in the surface area as shown in Fig. 2(b), when adopting the extended Thomas-Fermi approximation in the nucleon kinetic-energy density in which the SRC effects also were incorporated. The reason is that protons have larger values of the Weizsäcker surface term $(\nabla\rho_J/\rho_J)^2$. To evaluate the surface term, we adopt here the specified nucleon's density profile Eq. (1) by adjusting the diffuseness parameter of neutron density to obtain different neutron skin thicknesses for ^{208}Pb as shown in Fig. 2(a), in which the profile and numerical value are almost the same with that shown in Fig. 1(a). Therefore, according to Eq. (3), we have approximately in the surface area $k_{p/n}(r) \approx 1/(72M)(\nabla\rho_{p/n}/\rho_{p/n})^2 \approx 1/(72Ma^2_{p/n})$, leading to $k^{\rm loc}_p(r) > k^{\rm loc}_n(r)$ since the protons' surface diffuseness a_p is normally much less than the a_n for neutrons in heavy nuclei. From Figs. 2(a) and 2(b), more interestingly, we can see that the coexistence of a proton skin in k space and a neutron skin in r space reappeared as shown in Ref. [34]. In the current extended Thomas-Fermi approximation, the SRC effects were mainly included in the first term of the nucleon kinetic-energy density. It makes the local momenta of protons increase slightly even closer to that of neutrons in the interior area of the nucleus.

In order to avoid the hadronic probes, interacteractions with the nuclear medium that hinder the clean determination of neutron skin, hard photons, which are a promising probe for neutron skin, are studied. Figure 3 shows effects of proton skin in k space and neutron skin in r space on the time evolutions of hard photons with energies of $E_\gamma = 100$, 150, 200, and 250 MeV, respectively, in peripheral collisions ^{208}Pb + ^{208}Pb at $E_b = 45$ MeV/nucleon with impact parameter $b = 11$ fm. It also shows that the photon production with the thicker neutron skin is less than that with the thinner neutron skin especially for those of higher energy photons. This is because the larger neutron densities inside the thicker neutron skin get less photon emission through incoherent proton-neutron bremsstrahlung $p + n \to p + n + \gamma$ processes in the peripheral collisions of ^{208}Pb + ^{208}Pb, especially for emitting higher energy photons. However, effects of proton skin in k space on the hard photon emission are more pronounced than that of the neutron skin in r space. We can see that it gets more emissions of hard photons when considering the proton skin effect (mainly caused by the surface term in the nucleon kinetic-energy density) than without considering it except in the hard photon energy $E_\gamma = 250$ MeV. The surface term induces larger local momentum for the proton than that for the neutron in the surface area of the nucleus, which will increase the emission probability of hard photons through

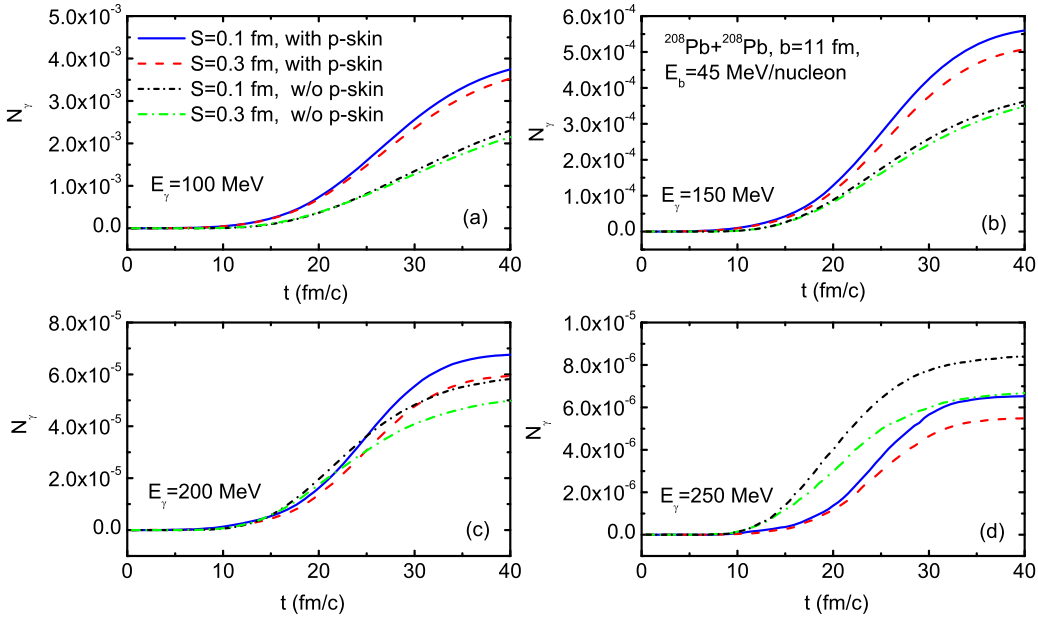

FIG. 3. Effects of the neutron skin in r space and proton skin in k space on multiplicity of hard photons with energies of $E_\gamma = 100$, 150, 200, and 250 MeV, respectively, in peripheral collisions $^{208}\mathrm{Pb} + ^{208}\mathrm{Pb}$ at a beam energy of 45 MeV/nucleon.

$p + n \to p + n + \gamma$ processes. The hard photon with energy $E_\gamma = 250$ MeV may originate from a multiple scattering of nucleons below Fermi momentum rather than from collisions of nucleons at HMT. It is not affected by the surface terms of the nucleon kinetic-energy density in which the short-range correlations are included.

Shown in Fig. 4 are angular distributions of the single differential probability of hard photons with energies of $E_\gamma = 100, 150, 200,$ and 250 MeV, respectively, in the c.m. frame of the colliding nuclei. We can see that the peak around $\theta = 90^\circ$ for the angular distribution of hard photons is reproduced as shown in Ref. [64]. Here, effects of the neutron skin in r space and proton skin in k space on the angular distribution of hard photons in peripheral collisions $^{208}\mathrm{Pb} + ^{208}\mathrm{Pb}$ at a beam energy of 45 MeV/nucleon are compared. With an increasing of hard photon energies, the effect of the neutron skin on the production of hard photons increases. Apparently, the thinner neutron skin creates more collision opportunities

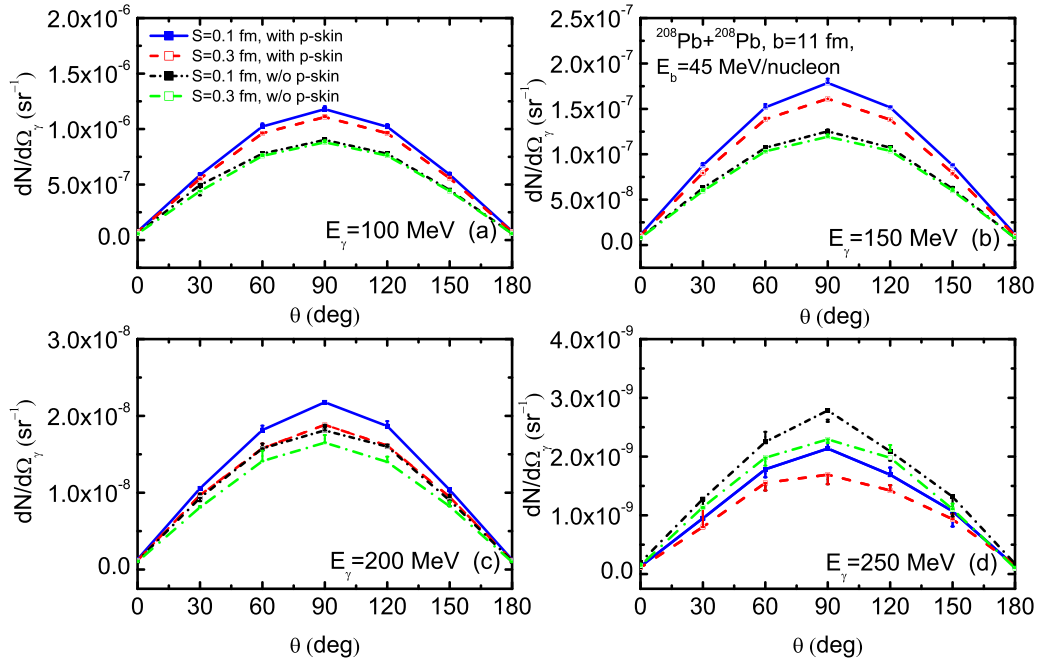

FIG. 4. Effects of the neutron skin in r space and proton skin in k space on the angular distributions of photons with energies of $E_\gamma = 100$, 150, 200, and 250 MeV in the c.m. frame of the colliding nuclei from peripheral $^{208}\mathrm{Pb} + ^{208}\mathrm{Pb}$ collisions at $E_b = 45$ MeV/nucleon.

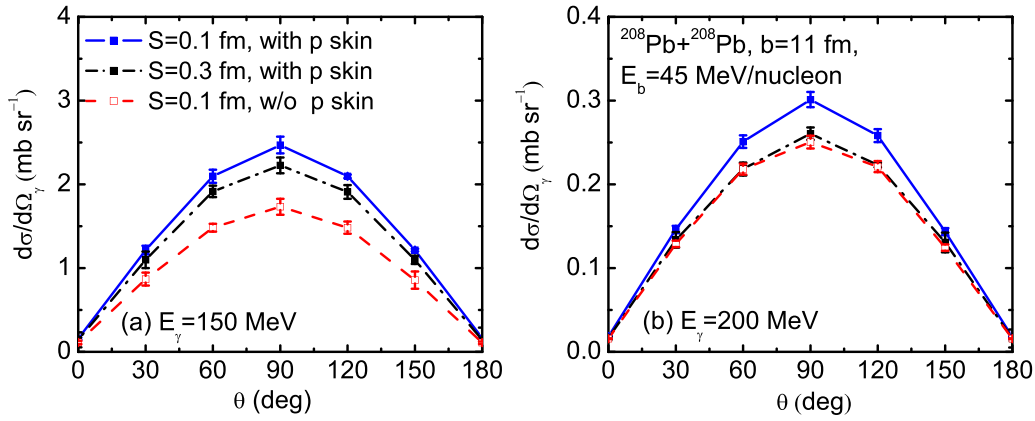

FIG. 5. Effects of the neutron skin in r space and proton skin in k space on the cross section of hard photons with energies of $E_\gamma = 150$ and 200 MeV in the c.m. frame of the colliding nuclei from peripheral $^{208}\mathrm{Pb} + ^{208}\mathrm{Pb}$ collisions at $E_b = 45$ MeV/nucleon.

for neutrons and protons from $p + n \to p + n + \gamma$ processes in the peripheral collisions, which will make more energetic hard photons. Moreover, the effect of the neutron skin on the emission of hard photons becomes larger when considering the proton skin in k space. This is because the increasing local momentum of protons near the surface of the nucleus creates more colliding for protons with neutrons with neutron skin of $S = 0.3$ fm compared with neutron skin of $S = 0.1$ fm in the heavy-ion reactions. As obtained in Fig. 3, effects of proton skin in k space on the angular distribution of hard photons are also more pronounced than those of the neutron skin in r space. Thus, it will strongly interfere with the determination of the size of the neutron skin.

To provide more basis for experimentalists measuring hard photons better, the distributions of cross sections for hard photon production with polar angular in the c.m. frame of the colliding nuclei are shown in Fig. 5. The same as before, the cross section of hard photons with energies 150 and 200 MeV in $^{208}\mathrm{Pb} + ^{208}\mathrm{Pb}$ at a beam energy of $E_b = 45$ MeV/nucleon with different neutron skins in r space and with or without proton skins in k space are compared. From Figs. 5(a) and 5(b), we can see that effects of the proton skin in k space on the cross section of hard photons are larger than that of the neutron skin in r space. More quantitatively, the effect of proton skin on the cross section of hard photons at $E_\gamma = 150$ MeV is about 3 times that of the neutron skin, and 1.25 times at $E_\gamma = 200$ MeV at $\theta = 90^\circ$. The effect of the proton skin on the cross section of hard photons at $E_\gamma = 200$ MeV becomes smaller on account of the part of the hard photons with higher energy coming from multiple scattering of nucleons below Fermi momentum which are not affected by the surface term of the nucleon energy density.

Figure 6(a) describes the transverse momentum distributions of the hard photons spectra, $dN/p_t dp_t$ versus p_t ($p_t = \sqrt{p_x^2 + p_y^2}$) in the midrapidity region of $-0.4 \leqslant y_0 \leqslant 0.4$ ($y_0 = y/y_{\mathrm{beam}}$ is the ratio of particle rapidity y over beam rapidity y_{beam} in the c.m. frame of colliding nuclei), for peripheral collisions of $^{208}\mathrm{Pb} + ^{208}\mathrm{Pb}$ at a beam energy of $E_b = 45$ MeV/nucleon with different neutron skins in r space and with or without proton skins in k space. It is seen that the spectra

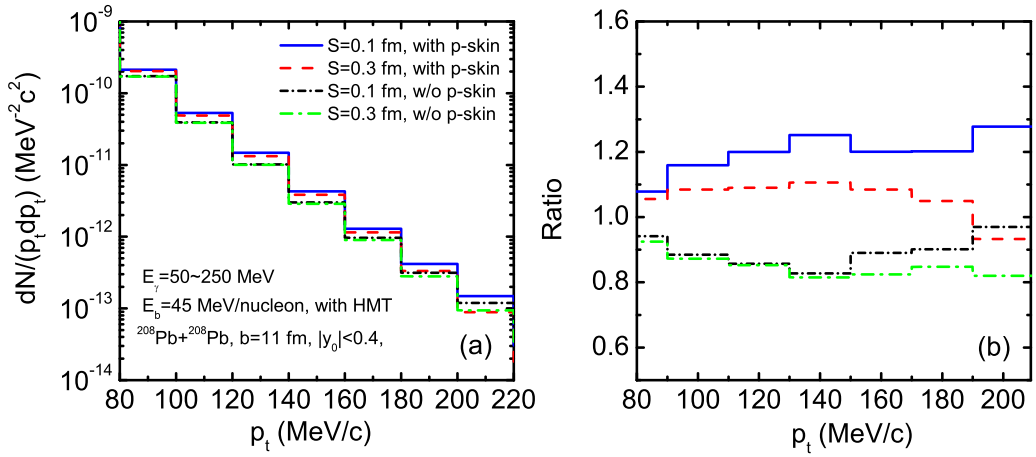

FIG. 6. Effects of the neutron skin in r space and proton skin in k space on the transverse momentum dependence of hard photons (a) and ratios of each transverse momentum spectrum of hard photons and average value of the transverse momentum spectra for four cases (b) in the midrapidity region of $-0.4 \leqslant y_0 \leqslant 0.4$ in peripheral $^{208}\mathrm{Pb} + ^{208}\mathrm{Pb}$ collisions at $E_b = 45$ MeV/nucleon.

show typical exponential shapes considering different neutron skins and proton skins. Interestingly, when considering the proton skin in k space, effects of the different neutron skins on the transverse momentum spectrum are more obvious compared to without considering it especially at high transverse momentum. This is the same with the conclusion shown in Figs. 3 and 4. To evaluate the specific effects of both neutron skin in r space and proton skin in k space on the transverse momentum spectrum of hard photons, shown in Fig. 6(b) are the ratios of each transverse momentum spectrum of hard photons in Fig. 6(a) over the average value of the transverse momentum spectra for four cases. We can clearly see that the effect of neutron skin on the above ratio of transverse momentum spectra of hard photons becomes larger with the increase of the transverse momentum. Moreover, from the mentioned ratios of transverse momentum spectra of hard photons for different neutron skins and proton skins, we found that it is more sensitive to the proton skin in k space than to the neutron skin in r space. Thus, the effect of proton skins in k space is not a negligible factor, when determining the size of neutron skin by the emission of hard photons. Interestingly, the effect of proton skin on the ratio of transverse momentum spectra of hard photons is more obvious than that on the angular distributions of hard photons, making the former a promising observable for investigating the surface properties of the nucleus.

IV. SUMMARY AND OUTLOOK

Motivated by the new efforts in better understanding and/or measuring the neutron skin thickness of nuclei, as well as the strong interests of some experimental groups to measure hard photons [65–67], we studied the interplay of the effects of neutron skins in coordinate space and proton skins in momentum space on hard photons emission in the neutron-rich reaction $^{208}\mathrm{Pb} + ^{208}\mathrm{Pb}$ around Fermi energy. In this work, we adopt the extended Thomas-Fermi approximation for the nucleon kinetic-energy density, in which the SRC effects were incorporated, in the IBUU transport model. Here, the coexistence phenomenon of the proton skins in k space and the neutron skin in r space exists as shown in Ref. [34]. It is found that the hard photon production with thinner neutron skin ($S = 0.1$ fm) is larger than that with thicker neutron skin ($S = 0.1$ fm) in peripheral collisions especially for those of higher energy photons. With an increasing of the hard photon energies, the effect of neutron skins on the emission of the hard photons increases. Therefore, the production of hard photons from peripheral heavy-ion collisions is a good probe to investigate the size of neutron skin with its characteristics unaltered by final state interactions. Moreover, it is noticed that the effect of neutron skin in r space on the emission of hard photons becomes larger when considering the surface term in the kinetic energy density, leading to the appearance of a proton skin in k space. It reminds us to consider effects of proton skins when determining the size of neutron skins by the production of hard photons. In addition, the angular distributions of the single differential probability and the transverse momentum spectrum for hard photons in peripheral collisions of $^{208}\mathrm{Pb} + ^{208}\mathrm{Pb}$ at a beam energy 45 MeV/nucleon were studied in this work. It will provide a basis for the ongoing and planned experiments using hard photons to explore the initial stage in intermediate energy heavy-ion collisions.

To this end, it is necessary to emphasize that our work presented here has caveats and more work is necessary to address them properly. There are actually many other parameters/aspects besides the neutron skin in coordinate and proton skin in momentum in the initial state of the projectile and target in transport model simulations of their collisions, such as the size, shape, and isospin dependence of the SRC/HMT; the momentum and density dependence of the symmetry potential and the associated neutron-proton effective mass splitting; as well as the in-medium NN collision cross sections, which may impact the hard photon observable. While our present and previous works as well as those by others have studied individually some of the uncertainties associated with these physics ingredients, there are some systematic uncertainties in our model predictions that we cannot presently address properly. Nevertheless, we do plan to carry out a comprehensive analysis to access the uncertainties and correlations of the major uncertain variables/aspects involved in transport model simulations of hard photon production in intermediate energy heavy-ion collisions. For this purpose, a covariance analysis similar to the work in Ref. [68] or a Bayesian inference once enough relevant experimental data become available similar to the work in Ref. [69] may be useful.

ACKNOWLEDGMENTS

The work is partially supported by the the Key Program of Anhui Provincial University Research Projects under Grant No. 2023AH050147, the Key Program of Innovation and Entrepreneurship Support Plan for Returned Talents in Anhui Province under Grant No. 2020LCX011, and the Institute of Energy, Hefei Comprehensive National Science Center under Grant No. GXXT-2020-004. B.A.L. is supported in part by the U.S. Department of Energy, Office of Science, under Award No. DE-SC0013702, the CUSTIPEN (China-U.S. Theory Institute for Physics with Exotic Nuclei) under U.S. Department of Energy Grant No. DE-SC0009971.

[1] B. Alex Brown, Phys. Rev. Lett. **85**, 5296 (2000).
[2] Brendan T. Reed, F. J. Fattoyev, C. J. Horowitz, and J. Piekarewicz, Phys. Rev. Lett. **126**, 172503 (2021).
[3] M. Centelles, X. Roca-Maza, X. Viñas, and M. Warda, Phys. Rev. Lett. **102**, 122502 (2009).
[4] X. Roca-Maza, M. Centelles, X. Viñas, and M. Warda, Phys. Rev. Lett. **106**, 252501 (2011).
[5] A. Trzcińska, J. Jastrzębski, P. Lubiński, F. J. Hartmann, R. Schmidt, T. vonEgidy, and B. Klos, Phys. Rev. Lett. **87**, 082501 (2001).

[6] J. Jastrzębski, A. Trzcińska, P. Lubiński *et al.*, Int. J. Mod. Phys. E **13**, 343 (2004).
[7] C. J. Horowitz, K. S. Kumar, and R. Michaels, Eur. Phys. J. A **50**, 48 (2014).
[8] S. Abrahamyan *et al.* (PREX Collaboration), Phys. Rev. Lett. **108**, 112502 (2012).
[9] D. Adhikari *et al.* (PREX Collaboration), Phys. Rev. Lett. **126**, 172502 (2021).
[10] L. W. Chen, C. M. Ko, and B. A. Li, and J. Xu, Phys. Rev. C **82**, 024321 (2010).
[11] P.-G. Reinhard, X. Roca-Maza, and W. Nazarewicz, Phys. Rev. Lett. **127**, 232501 (2021).
[12] B. S. Hu, W. G. Jiang, T. Miyagi *et al.*, Nat. Phys. **18**, 1196 (2022).
[13] P. Danielewicz, Nucl. Phys. A **727**, 233 (2003).
[14] J. Zenihiro, H. Sakaguchi, T. Murakami *et al.*, Phys. Rev. C **82**, 044611 (2010).
[15] B. Kłos, A. Trzcińska, J. Jastrzebski, T. Czosnyka, M. Kisielinski, P. Lubinski, P. Napiorkowski, L. Pienkowski, F. J. Hartmann, B. Ketzer, P. Ring, R. Schmidt, T. von Egidy, R. Smolanczuk, S. Wycech, K. Gulda, W. Kurcewicz, E. Widmann, and B. A. Brown, Phys. Rev. C **76**, 014311 (2007).
[16] T. Z. Yan and S. Li, Nucl. Sci. Tech. **30**, 43 (2019).
[17] X. Y. Sun, D. Q. Fang, Y. G. Ma *et al.*, Phys. Lett. B **682**, 396 (2010).
[18] G. F. Wei, B. A. Li, J. Xu, and L. W. Chen, Phys. Rev. C **90**, 014610 (2014).
[19] H. L. Li, H. J. Xu, Y. Zhou, X. B. Wang, J. Zhao, L. W. Chen, and F. Q. Wang, Phys. Rev. Lett. **125**, 222301 (2020).
[20] J. Hammelmann, A. Soto-Ontoso, M. Alvioli, H. Elfner, and M. Strikman, Phys. Rev. C **101**, 061901(R) (2020).
[21] G. Giacalone, G. Nijs, and W. van der Schee, arXiv:2305.00015.
[22] G. C. Yong, B. A. Li, and L. W. Chen, Phys. Lett. B **661**, 82 (2008).
[23] G. Giuliani and M. Papa, Phys. Rev. C **73**, 031601(R) (2006).
[24] E. L. Reber, K. W. Kemper, P. V. Green, P. L. Kerr, A. J. Mendez, E. G. Myers, and B. G. Schmidt, Phys. Rev. C **49**, R1 (1994).
[25] T. Biro, K. Niita, A. D. Paoli, W. Bauer, W. Cassing, and U. Mosel, Nucl. Phys. A **475**, 579 (1987).
[26] W. Bauer, G. F. Bertsch, W. Cassing, and U. Mosel, Phys. Rev. C **34**, 2127 (1986).
[27] G. H. Liu, Y. G. Ma, X. Z. Cai, D. Q. Fang, W. Q. Shen, W. D. Tian, and K. Wang, Phys. Lett. B **663**, 312 (2008).
[28] G. C. Yong and B. A. Li, Phys. Rev. C **96**, 064614 (2017).
[29] G. F. Wei, Phys. Rev. C **92**, 014614 (2015).
[30] S. S. Wang, Y. G. Ma, D. Q. Fang, and X. G. Cao, Phys. Rev. C **105**, 034616 (2022).
[31] J. Arrington *et al.*, Prog. Part. Nucl. Phys. **67**, 898 (2012).
[32] C. Ciofi degli Atti, Phys. Rep. **590**, 1 (2015).
[33] O. Hen, G. A. Miller, E. Piasetzky, and L. B. Weinstein, Rev. Mod. Phys. **89**, 045002 (2017).
[34] B. J. Cai, B. A. Li, and L. W. Chen, Phys. Rev. C **94**, 061302(R) (2016).
[35] A. Sorensen, K. Agarwal, K. W. Brown, Z. Chajecki, P. Danielewicz, C. Drischler, S. Gandolfi, J. W. Holt, M. Kaminski, C. M. Ko *et al.*, arXiv:2301.13253.
[36] B. A. Li, C. B. Das, S. Das Gupta, and C. Gale, Phys. Rev. C **69**, 011603(R) (2004); Nucl. Phys. A **735**, 563 (2004).
[37] B. A. Li, G. C. Yong, and W. Zuo, Phys. Rev. C **71**, 014608 (2005).
[38] A. GomezCamacho, N. Yu, H. Q. Zhang, P. R. S. Gomes, H. M. Jia, J. Lubian, and C. J. Lin, Phys. Rev. C **91**, 044610 (2015).
[39] K. S. A. Hassaneen and H. Müther, Phys. Rev. C **70**, 054308 (2004).
[40] A. Rios, A. Polls, and W. H. Dickhoff, Phys. Rev. C **89**, 044303 (2014).
[41] Z. H. Li and H. J. Schulze, Phys. Rev. C **94**, 024322 (2016).
[42] J. T. Stewart, J. P. Gaebler, T. E. Drake, and D. S. Jin, Phys. Rev. Lett. **104**, 235301 (2010).
[43] I. Tews, T. Krüger, K. Hebeler, and A. Schwenk, Phys. Rev. Lett. **110**, 032504 (2013).
[44] A. Gezerlis, I. Tews, E. Epelbaum, S. Gandolfi, K. Hebeler, A. Nogga, and A. Schwenk, Phys. Rev. Lett. **111**, 032501 (2013).
[45] A. Schwenk and C. J. Pethick, Phys. Rev. Lett. **95**, 160401 (2005).
[46] E. Epelbaum *et al.*, Eur. Phys. J. A **40**, 199 (2009).
[47] A. Gezerlis and J. Carlson, Phys. Rev. C **81**, 025803 (2010).
[48] O. Hen, L. B. Weinstein, E. Piasetzky, G. A. Miller, M. M. Sargsian, and Y. Sagi, Phys. Rev. C **92**, 045205 (2015).
[49] O. Hen *et al.*, Science **346**, 614 (2014).
[50] B. A. Li, B. J. Cai, L. W. Chen, and J. Xu, Prog. Part. Nucl. Phys. **99**, 29 (2018).
[51] C. F. von Weizsäcker, Z. Phys. **96**, 431 (1935).
[52] M. Brack, C. Guet, and H. B. Hakansson, Phys. Rep. **123**, 275 (1985).
[53] S. V. Lucyanov and A. I. Sanzhur, Nucl. Phys. At. Energy **17**, 5 (2016).
[54] C. B. Das, S. Das Gupta, C. Gale, and B. A. Li, Phys. Rev. C **67**, 034611 (2003).
[55] W. Cassing, V. Metag, U. Mosel, and K. Niita, Phys. Rep. **188**, 363 (1990).
[56] H. Xue, C. Xu, G.-C. Yong, and Z. Ren, Phys. Lett. B **755**, 486 (2016).
[57] G. C. Yong, Phys. Lett. B **776**, 447 (2018).
[58] Y. Schutz *et al.* (TAPS Collaboration), Nucl. Phys. A **622**, 404 (1997).
[59] G. F. Bertsch and S. Das Gupta, Phys. Rep. **160**, 189 (1988).
[60] K. Nakayama and G. F. Bertsch, Phys. Rev. C **34**, 2190 (1986).
[61] M. Schäfer, T. S. Biro, W. Cassing, U. Mosel, H. Nifenecker, and J. A. Pinstan, Z. Phys. A **339**, 391 (1991).
[62] R. G. E. Timmermans, T. D. Penninga, B. F. Gibson, and M. K. Liou, Phys. Rev. C **73**, 034006 (2006).
[63] J. Friedrich and P. G. Reinhard, Phys. Rev. C **33**, 335 (1986).
[64] W. M. Guo, B. A. Li, and G. C. Yong, Phys. Rev. C **104**, 034603 (2021).
[65] A. B. McIntosh, G. Verde, and Z.-G. Xiao (private communications).
[66] Y. Qin, Q. Niu, D. Guo, S. Xiao, B. Tian, Y. Wang, Z. Qin, X. Diao, F. Guan, and D. Si *et al.*, arXiv:2307.10717 [nucl-ex].
[67] D. Si, Y. Zhou, S. Xiao, and Z. Xiao, arXiv:2307.12995 [physics.ins-det].
[68] Y. X. Zhang, M. B. Tsang, and Z. X. Li, Phys. Lett. B **749**, 262 (2015).
[69] B. A. Li and W. J. Xie, Nucl. Phys. A **1039**, 122726 (2023).